Closed-Loop Control Simulations on a Morphing Wing

Andrei Vladimir Popov,* Michel Labib,† Julien Fays,‡ and Ruxandra Mihaela Botez§
École de Technologie Supérieure, Montréal, Québec H3C 1K3, Canada

The main objective of the project is to develop a system for the active control of wing airfoil geometry during flight to allow drag reduction. Drag reduction on a wing can be achieved by modifications in the laminar to turbulent flow transition point position, which should move toward the trailing edge of the airfoil wing. As the transition point plays a crucial part in this project, this paper focuses on the control of its position on the airfoil, as an effect of the deflection control on a morphing wing airfoil equipped with a flexible skin. The reference airfoil is the laminar WTEA-TE1 airfoil, on which a flexible skin is located; its geometry is modified by the use of a single point control, where it is assumed that one actuator acts. The Mach number, angle of attack, and deflection allow us to calculate the pressures and transition point positions at each step. The varying inputs are the deflections and the angles of attack. As they both change, the transition point position changes accordingly. A model of a shape memory alloy has been carried out in the MATLAB®/Simulink environment. Hence, the challenge is to perform the control with a shape memory alloy in the closed loop, as it has a nonlinear behavior. Several controllers, such as a proportional integral derivative controller, a proportional controller, and variables gains, are therefore necessary to control the shape memory alloy and the entire closed loop. Three simulations have been carried out to validate the control. The first simulation keeps the angle of attack constant and is performed for successive deflections. The second simulation considers different steps for the deflection but adds a sinusoidal component for the angle of attack; this simulation is closer to the cruise flight regime. During the third simulation, both the angle of attack and the deflection are modeled as a sinusoidal wave. The outputs (the deflection and the transition point position) are well controlled and the results are very good. Hence, it is concluded that this original method of control is suitable for the control of the transition point position from the laminar to turbulent region on a morphing wing airfoil.

Nomenclature

F	=	applied force on the shape memory alloy
i	=	current in the shape memory alloy
K	=	static gain of the proportional integral derivative
K_c	=	critical gain of the proportional integral derivative
K_d	=	derivative gain of the proportional integral derivative
K_i	=	integral gain of the proportional integral derivative
K_p	=	proportional gain of the proportional integral derivative
M	=	Mach number
Re	=	Reynolds number
T_c	=	critical period of the shape memory alloy model
T_i	=	initial temperature in the shape memory alloy
α	=	angle of attack
τ_c	=	controller delay of the proportional integral derivative controlling the shape memory alloy model
τ_1	=	time delay of the proportional integral derivative controlling the shape memory alloy model
τ_2	=	time delay of the proportional integral derivative controlling the shape memory alloy model
τ_3	=	dead time of the proportional integral derivative controlling the shape memory alloy model

I. Introduction

INCREASES in fuel prices are burning issues that represent the main challenges in the aeronautical field. In the aerospace industry, these issues may be solved by fuel consumption reduction,

*Ph.D. Student; andrei-vladimir.popov.1@ens.etsmtl.ca. Member AIAA.
†Master's Student; michel.labib.1@ens.etsmtl.ca. Member AIAA.
‡Internship Student; jfays@estaca.fr. Member AIAA.
§Professor, 1100 Notre Dame West; ruxandra@gpa.etsmtl.ca. Member AIAA.

translated in drag reduction, through a most efficient wing design. To achieve this design, there is the need to obtain a larger part of the laminar flow on the wing, which is equivalent to the transition point displacement toward the trailing edge.

One method of laminar flow improvement studied wing geometry modification by inflating and deflating installed bumps at a certain frequency. Munday et al. [1] used piezoelectric actuators to inflate and deflate bumps on the upper surface of wings in a wind tunnel to determine the transition point displacement. Turbulent flow was thus delayed and the lift coefficient was increased by up to 7%. The flow active control was therefore achieved by modifying the wing geometry.

Another laminar flow study method concerned wing geometry modification by installation and optimization of a bump on the upper surface of the airfoil to improve shock wave control in transonic flow [2]. Optimization of this bump gave a 70% reduction in friction drag and a 15% reduction in the total drag on the wing. Because the bump optimization required a high number of iterations during the numerical aerodynamic analysis, the Euler 2-D code with a boundary-layer correction was chosen to save time. The flow around the optimized wing geometry was studied using a Navier–Stokes code.

Sobieczky and Geissler [3] simulated the behavior of a wing configured with one bump at the leading edge and a second bump at the trailing edge of the upper surface for Mach numbers ranging from 0.72 to 0.77. The results showed a drag reduction of 10%.

Yet another method is the modification of the geometry by leading- and trailing-edge variations. Martins and Catalano [4] studied drag reduction on adaptive wings for a transport aircraft manufactured by Embraer Aircraft Company. The camber of the adaptive wing airfoil was modified to deform the leading and the trailing edge of the airfoil. The panel method with a boundary-layer correction was used. The transition point moved at 40% from the airfoil chord (instead of 10%), and the friction drag was reduced by 24%.

Powers and Webb [5] performed various flight tests at the NASA Dryden Flight Research Center on an F-111 aircraft. Their results were useful for numerical aerodynamics code validation and showed

an increase in the lift coefficient dependent on the wing airfoil geometry modification.

Fiber Bragg gratings (FBGs) were applied to measure dynamic strains inside a subscale wing during a real-time wind-tunnel test [6]. Two recoated FBGs were embedded in the wing skin. The FBG sensor system included a wavelength-swept fiber laser with a wavelength indicator and fast signal processing modules. The agreement among the three sensor types inside the subscale wing (FBG, electric strain gauge, and lead zirconate titanate) was confirmed in a bench test. The optical fiber strain sensors had excellent resolution in the time domain and could detect a frequency response of up to 100 Hz.

In [6], two 16% scale wind-tunnel models, the first one conventional and the other incorporating smart wing design features, were designed and manufactured at NASA for Langley's 16 ft Transonic Dynamic Tunnel. Two series of tests were conducted to evaluate the advantages of the smart wing concept. A key objective of the Smart Wing Phase 1 program was to identify and reduce the risks involved with the integration of smart materials into an actual flight vehicle. The following topics were studied: 1) model design and static testing requirements, 2) design and manufacturing of the shape memory alloy (SMA) control surfaces, 3) system integration, and 4) posttest analysis and planned improvements. Lessons learned from the Phase 1 efforts were discussed along with plans for the Smart Wing Phase 2 program [7].

From the existing literature, there is no controller design using SMAs to move the transition point closer to the trailing edge to improve the laminar flow on a wing. To achieve this goal for the first time, a new algorithm was conceived to determine the transition point positions from the detection of a sudden increase in pressure. This algorithm, presented in a previous paper [8], used the Xfoil code results obtained in terms of lift, drag, pressure coefficients, and transition point positions vs the laminar airfoil chord to determine the transition point positions from the pressure distribution simulated with the Xfoil code. It was concluded, because intermediate pressure coefficients for intermediate airfoils could be calculated adequately by use of this new algorithm, that the transition point positions could be determined from wind-tunnel pressure measurements in real time in which airfoil shapes change for various flow conditions characterized by Mach numbers, Reynolds numbers, and angles of attack. A computational fluid dynamics (CFD) database was built for a range of airflow parameters and, by use of this new algorithm, the transition point position was calculated for intermediate wing airfoils and airflow parameters.

In this paper, the design aspects of a laminar flow controller on a wing equipped with flexible skin (localized at 7–65% of the airfoil chord) and an SMA were presented. The wing model built upon the concept shown in this paper, equipped with optical pressure sensors, a controller, and shape memory actuators will be tested in the near future in the wind tunnel. Figure 1 shows the scheme of the controller closed loop.

For a range of Mach numbers M, angles of attack, and Reynolds numbers Re (block 1 in Fig. 1), the upper surface of the airfoil is modified by use of an actuator located at a certain percentage of the chord where its corresponding deflection is obtained. The transition point positions were found from the detection of a sudden increase of pressure by use of the new algorithm [8] and shown in block 2 in Fig. 1.

Then, the controller (block 3 in Fig. 1) sends a command to the smart actuators (block 4 in Fig. 1) located on the flexible airfoil skin to change the wing shape and, therefore, to move the transition point

closer to the trailing edge, thus increasing the laminar flow region on the wing airfoil. As a consequence, the laminar flow region becomes more substantial than the turbulent flow region on the upper wing surface and drag coefficients are reduced, which lowers fuel consumption.

The reference airfoil considered in this paper is the laminar WTEA-TE1 airfoil, with its chord of 50 cm. The airfoil coordinates and its data expressed in terms of lift, drag, pressure coefficients, and transition point position vs the chord were validated experimentally in the wind tunnel and numerically with the XFoil code.

This reference airfoil is modified by use of a single control point localized at 36% of the chord, where it is assumed that one actuator acts, thus creating a deflection from -2 to $+2$ cm of the upper surface airfoil. Seventeen different airfoils are obtained by spline interpolation modifying the control point position while maintaining the tangency condition to the fixed points located at 7 and 65% of chord, which are shown in Fig. 2.

Details of block 2 (see Fig. 1) are shown in Fig. 3. The controller simulation and validation are performed here for the following airflow conditions: angles of attack, $\alpha = -2$ to $+2$ deg; Reynolds number $Re = 2.29 \times 10^6$; and Mach number, $M = 0.2$ (see Figs. 4–6). These airflow conditions were chosen due to the wind-tunnel airflow limitations. The maximum Mach number in the considered wind tunnel is $M = 0.35$.

II. Closed-Loop Controller Design

The controller goal mainly concerns the displacement of the transition point position closer to the trailing edge to produce a higher laminar flow region on the airfoil and, therefore, to control the airfoil deflection for all airflow conditions. The closed loop is composed of three main blocks, as shown in Fig. 1: update of pressure and transition point position values, block 5; SMA, block 4; and controller, block 3.

Each block is detailed in the following subsections.

A. Block 2: Determination of Pressure and Transition Point Position

Block 2 receives the values of the four inputs (shown in block 1 in Fig. 1) and calculates the values of th epressure coefficients vs the chord and transition point positions for airflow conditions with the new algorithm [8].

B. Block 5: Update of Pressure and Transition Point Position Values

Block 5 (in Fig. 1) is the same as block 2. Block 5 inputs are the angles of attack, the Mach numbers, and the percentage of the chord. The new value of deflection is obtained in block 5 with respect to block 2, for which the deflection is defined as the input. In block 5, the actual deflection is calculated as the output of the SMA block. Hence, block 5 realizes an update of the pressure and the transition point position. The actual pressure and the actual transition point position are therefore obtained at each simulation step.

C. Block 4: Shape Memory Alloy

The SMA block contains the model of the SMA, as shown in Fig. 7.

The goal of block 4 is to control the airfoil deflection located at 36% of the airfoil chord, created with an SMA. The proportional integral derivative (PID) controller sends a command to the SMA to change the airfoil shape, so that the transition point can move toward the trailing edge. The SMA's functioning principle is shown in
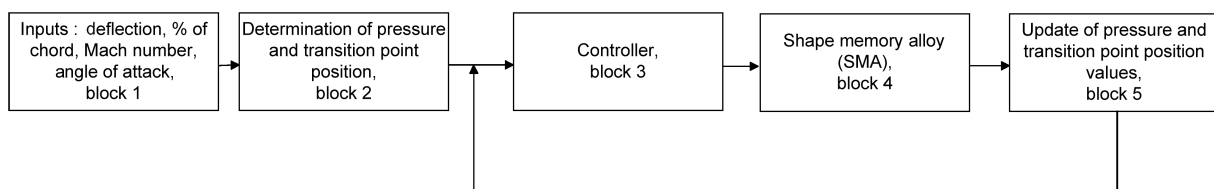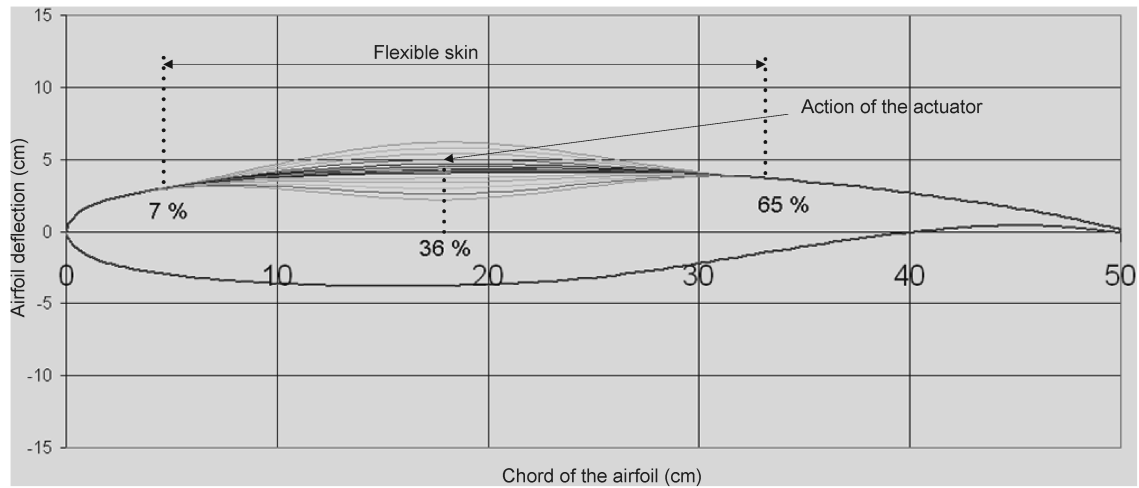

Fig. 1 Controller closed-loop scheme.

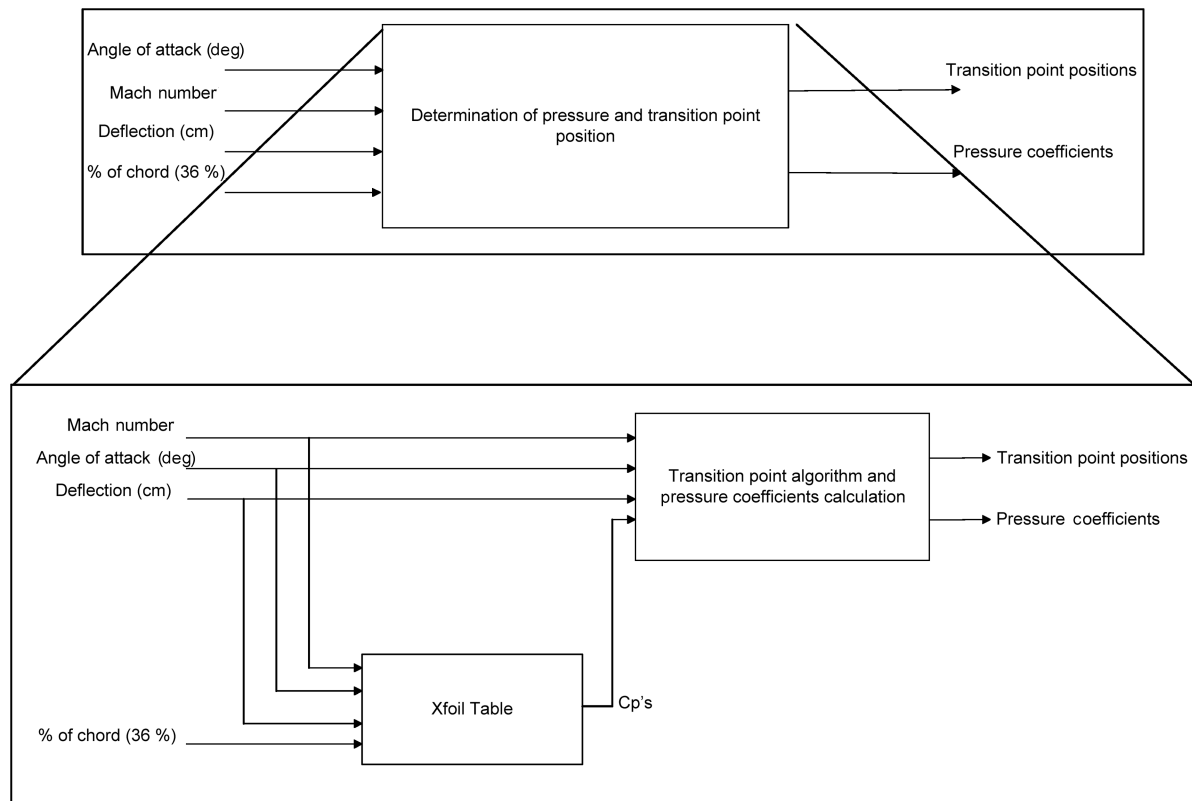**Fig. 2 WTEA-TE1 reference airfoil and its modified airfoils shapes.**

Fig. 3 Details of block 2: determination of the pressure coefficients vs the chord and transition point position [8].

Fig. 8. The shape memory actuators are manufactured from a Ti–Ni alloy wire. These alloys have the property of exhibiting martensitic transformation when they are deformed at a low temperature phase, and they recover their original shape after heating. In Fig. 8, an SMA wire loaded with a mass suspended at the ambient temperature is shown schematically. The load changes the internal forces between the atoms, forcing them to change their positions in the crystals and consequently forcing the wires to lengthen, which is called the SMA activation or the initial phase.

When the wire is heated by use of a current, the generated heat by the current resistivity causes the atoms in the crystalline structure to realign and force the alloy to recover its original shape. After that, any change in the internal temperature of the alloy will modify the crystalline structure accordingly and then the exterior shape of the wire. This property of changing the length of the wire as a function of

the electrical current that passes through the wire is used for actuation purposes. In this paper, a theoretical SMA model developed by Terriault [9] is used.

The three inputs of this model are the initial temperature $T_i = 380$ K (see Fig. 6), the current intensity i of the SMA, and the applied force F on the SMA. The model simulates the behavior of an SMA wire length of 0.081 m, which is stretched by a force of 400 N. The wire changes its length by the amount of heat produced by the current that passes through it. The model outputs are the final temperature and the SMA displacement. An SMA has a nonlinear behavior [10], due to the several phases characterizing its functioning, as shown in Fig. 9.

In this paper, a PID controller is designed to control the SMA. To use the shape-changing characteristics, the SMA needs to be initialized by an external force, which obliges it to go initially
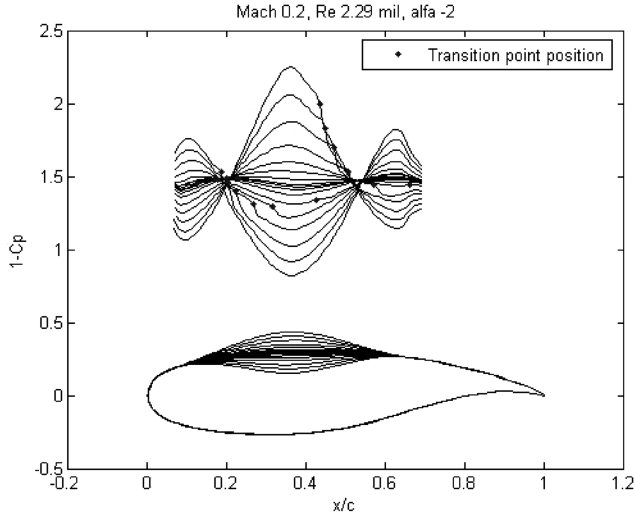
Fig. 4 Pressure coefficients vs the chord computed by Xfoil and the transition point position calculated by the new algorithm for Mach 0.2 and $\alpha = -2$ deg.
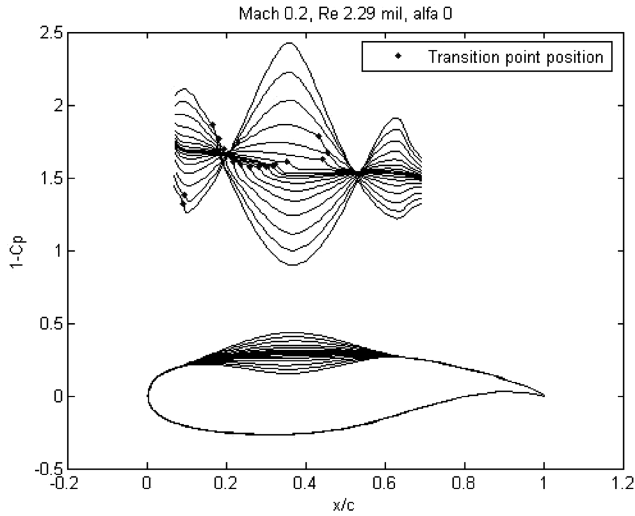

Fig. 5 Pressure coefficients vs the chord computed by Xfoil and the transition point position calculated by the new algorithm for Mach 0.2 and $\alpha = 0$ deg.
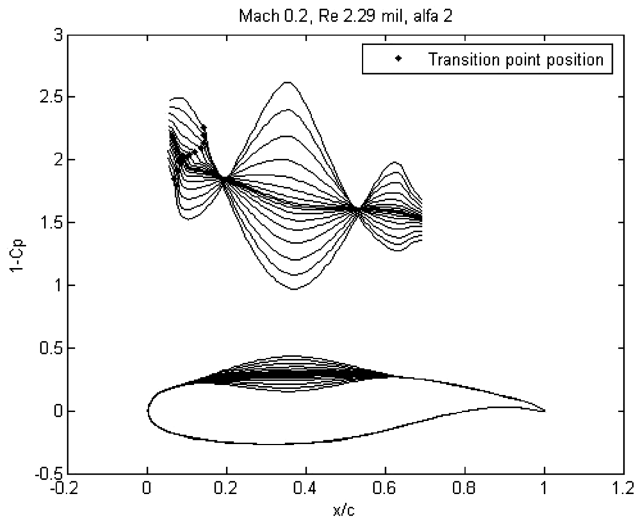

Fig. 6 Pressure coefficients vs the chord computed by Xfoil and the transition point position calculated by the new algorithm for Mach 0.2 and $\alpha = 2$ deg.

through the transformation phase and further to revert to the initial phase through the cooling phase. Before these two phases, the control can not be realized, due to the intrinsic behavior of the SMA.

Two methods are used to design the PID controller: the Ziegler–Nichols (ZN) method and the internal model control (IMC) method. These methods are described in Secs. II.C.1 and II.C.2.

1. Ziegler–Nichols Method [11]

A second-order transfer function $\frac{K}{(\tau_1 s + 1)(\tau_2 s + 1)} e^{\theta s}$ is obtained to approximate as much as possible the SMA open-loop model behavior. Hence, we realize an identification of its terms: the static gain K, the time delay τ_1, the time delay τ_2, and the dead time θ. This step is illustrated in Fig. 10.

The SMA has two phases associated with its behavior: a *cooling phase* and a *heating phase*. The following two transfer functions were found through parameter identification:

$$\text{TF}_{\text{cooling}} = \frac{0.0053}{(12s+1)(18s+1)} e^{13\ s} \quad \text{and} \quad \text{TF}_{\text{heating}} = \frac{0.0053}{(3s+1)(10s+1)} e^{17\ s},$$

corresponding to Fig. 11.

These transfer functions will be used to identify the parameters of the PID controller using the Ziegler–Nichols method.

This method allows for the determination of satisfactory values for each of the three gains (K_p, K_i, and K_d) present in the PID controller. K_p is the proportional gain, K_i is the integral gain, and K_d is the derivative gain. To find the values of K_p, K_i, and K_d, the first step is to determine the values of the critical gain K_c and the oscillating period T_c. Gains K_i and K_d are set to zero, and only K_p is used. Gain K_p is increased until the output starts to oscillate; when the output starts to oscillate, the critical gain K_c is found. We measure the value of K_c, as well as the period of oscillations T_c.

The second step is to use the values of K_c and T_c to find the correct values of K_p, K_i, and K_d. The following relationships are used to determine these gains [11]:

$$K_p = 0.6K_c, \qquad K_i = 2(K_p/T_c), \qquad K_d = K_p(T_c/8) \qquad (1)$$

Then, $K_p = 171$, $K_i = 6.22$, and $K_d = 1175.60$ are obtained.

The displacement of the actuator vs the temperature is shown in Fig. 11, whereas the displacement of the actuator vs the time is shown in Fig. 12.

The input is expressed as two successive steps. From $t = 0$ to 1000 s, the input remains at 0.0801 m. From $t = 1000$ to 3000 s, the first step input goes from 0.0801 to 0.0831 m. Then, from $t = 3000$ to 5000 s, the second step input goes from 0.0831 to 0.0822 m.

Initialization phase: This phase corresponds to the first 1000 s. It was found that the input and the output are not the same during this period of time. This difference comes from the intrinsic behavior of the SMA. Indeed, as seen in Fig. 6, the working point has to go through both the transformation and cooling phases before the action of any control on the SMA. This period of time can not be avoided, and the control can not be achieved until the working point reaches the end of the cooling phase. Once this period of time is over, the control can act precisely and give satisfactory results. A precision of 0.12% and a time response of 681 s at 0.5% of the input were found.

The precision is defined as

$$\text{precision}\ (\%) = \frac{|\text{output} - \text{input}|}{|\text{input}|} * 100 \qquad (2)$$

First step: At $t = 1000$ s, the input goes from 0.0801 to 0.0831 m. We found a precision of 0.02% and a time response of 374 s.

Second step: At $t = 3000$ s, the input goes from 0.0831 to 0.0822 m. We found a precision of 0.03% and a time response of 748 s.

2. Internal Model Control Method

The IMC [12] is another method to determine the values of the PID parameters. Two steps are followed in this method. The second step of the IMC method is to evaluate the K_p, K_i, and K_d gains by use of Eqs. (3) in a closed loop. The closed loop shown in Fig. 7 is considered, not the one shown in Fig. 1.
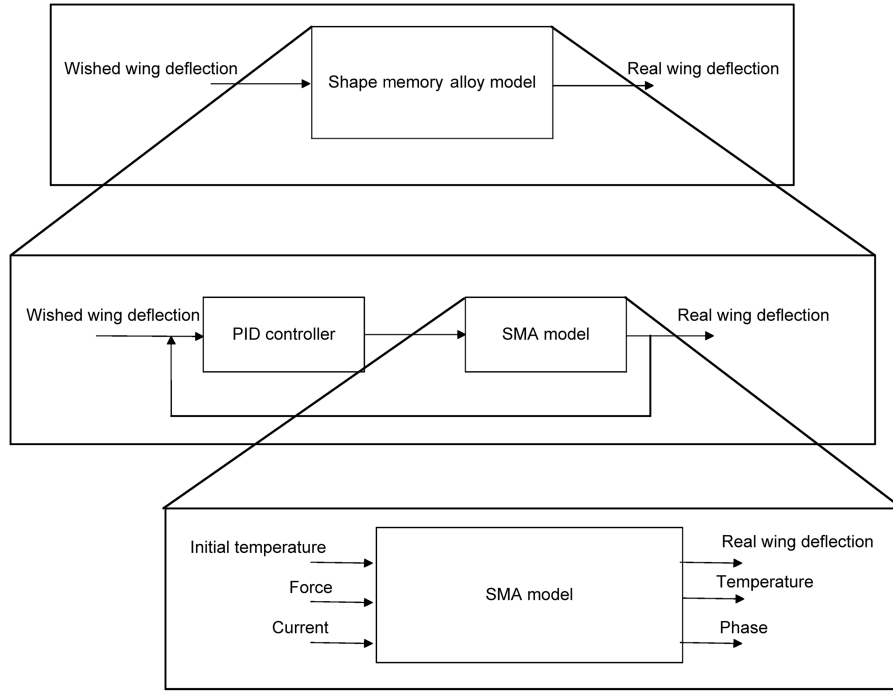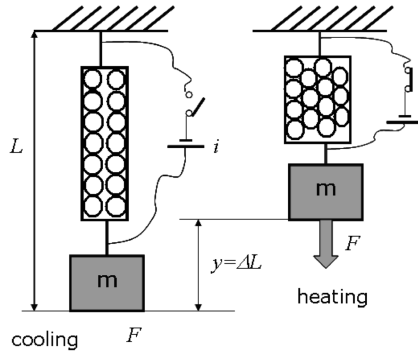
Fig. 7   Details of block 4: SMA.
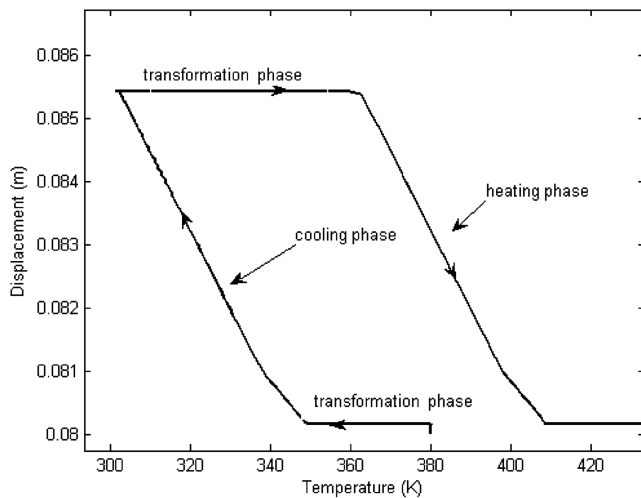

Fig. 8   SMA model scheme.

Fig. 9   SMA cycle.

$$K_p = \frac{\tau_1 + \tau_2}{K(\theta + \tau_c)}, \qquad K_i = \frac{1}{K(\theta + \tau_c)}, \qquad K_d = \frac{\tau_1 \tau_2}{K(\theta + \tau_c)} \quad (3)$$

The presence of the new term τ_c is noticed, which is the controller time delay, and is used in this method as an additional degree of freedom. Its value is modified to find the best control of the SMA

model. The actuator displacement vs the temperature and the actuator displacement vs the time are shown in Fig. 13 for several values of τ_c.

The same successive steps as the ones used for the ZN method are then enforced. The best value following different cases of τ_c is noticed in the case in which $\tau_c = 0$, showing the shortest time delay and shortest time response. Gains $K_p = 144.28$, $K_i = 11.10$, and $K_d = 332.96$ are hence obtained.

Initialization phase: This phase corresponds to the first 1000 s. The input and the output are not the same during this period. The difference between them comes from the intrinsic behavior of the SMA. Indeed, as seen in Fig. 9, the working point has to go through both the transformation and cooling phases before the action of any SMA control. This phase can not be avoided, and the control can not be achieved until the working point reaches the end of the cooling phase. Once this period is over, the control can act precisely and give satisfactory results. It was found a precision of 0.07% and a time response of 297 s.

First step: At $t = 1000$ s, the input goes from 0.0801 to 0.0831 m. We notice a precision of 0.09% and a time response of 208 s.

Second step: At $t = 3000$ s, the input goes from 0.0831 to 0.0822 m. We notice a precision of 0.23% and a time response of 381 s.

3.   Comparison of Results Obtained with Both Methods

To choose between these two methods, we can compare the obtained results on the same graph (see Fig. 14).

It is clear that the parameters K_p, K_i, and K_d found with the IMC method for $\tau_c = 0$ are better than the ones found with the ZN method. Even though the precision is a bit better with the ZN method, the time delay and time response is by far better with the IMC method, as shown in Table 1. It was decided to use the IMC method for the design of the PID controller.

4.   Control Improvement

Even though the controller works properly, it was decided to reduce the time response during the cooling phase. Indeed, the controller designed with the IMC method has a dead time θ, which creates a long time response, especially in the cooling phase. The idea here is to disconnect the controller action during the cooling phase, which means when the desired deflection is physically higher than the actual deflection. The controller action was disconnected with the
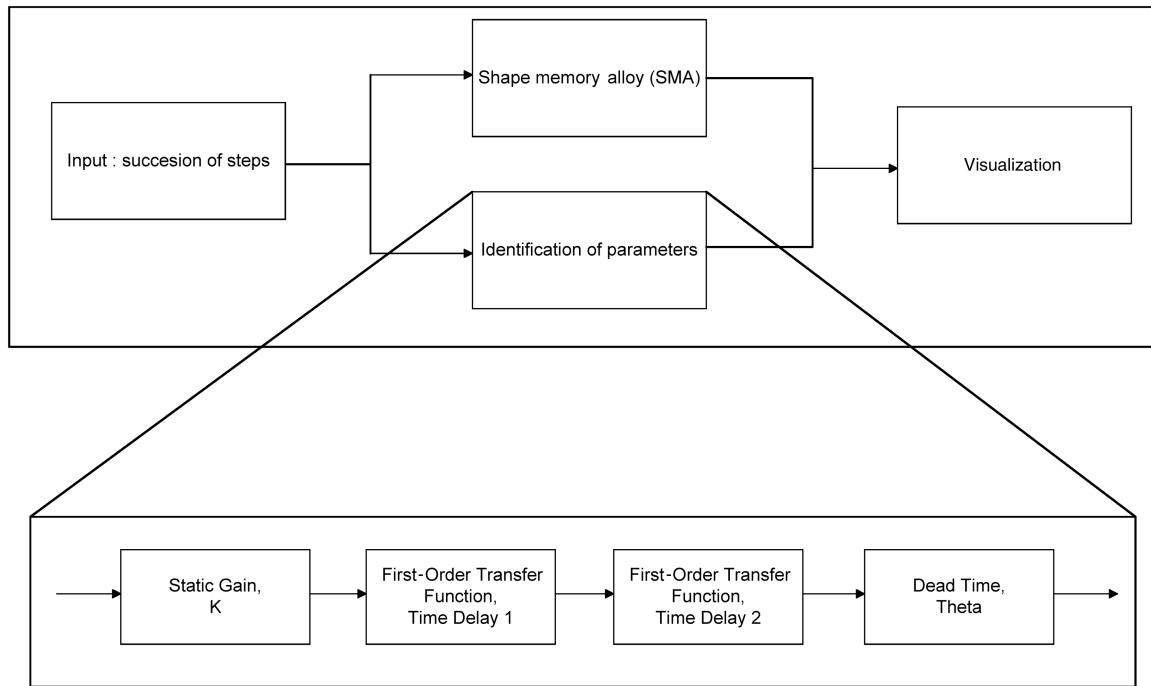
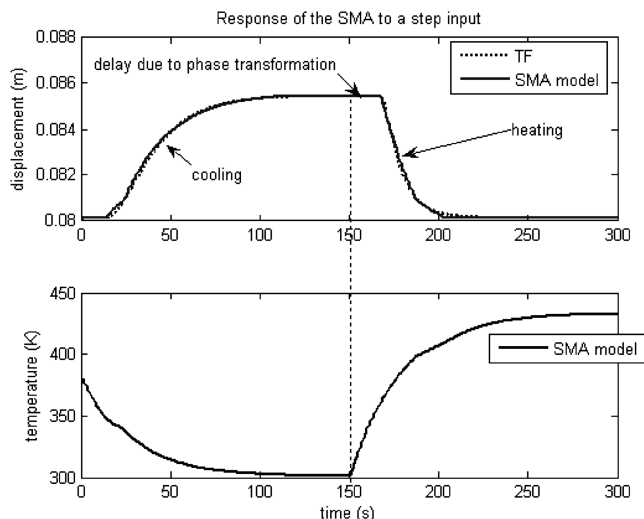**Fig. 10 Identification of the SMA's transfer functions.**

Fig. 11 Temperature and actuator displacement vs time with the SMA model compared with the corresponding transfer functions.

instruction $i = 0$ A in the SMA by use of the algorithm shown in Fig. 15.

The oscillations that appear are caused by the inertia of the SMA's heat transfer during the cooling and heating phase. Indeed, with a current of 0 A, the sign of the quantity "desired deflection minus actual deflection" continuously changes. Therefore, a switch was done continuously in our algorithm (Fig. 15), thus creating oscillations.

The goal of the "desired deflection superior to actual deflection" block is to control the airfoil deflection. It is located in the whole closed loop (Fig. 1), whereas the PID designed in the previous paragraph is only located in the SMA block.

Two types of closed-loop dynamics exist (Fig. 1). On one hand, we have a very fast dynamic in block 2 of Fig. 3, with our real-time algorithm that should react as fast as possible. On the other hand, in block 4 of Fig. 4, we have a very slow dynamic with very high time responses. For this reason, the PID controller located in the SMA block is not capable of controlling the whole closed loop of Fig. 1. It was thus necessary to create a controller block located before the SMA block in the closed loop to deal with those two dynamics. This controller block is composed of two types of gains: a fixed proportional gain and a variable gain. The proportional gain reduces
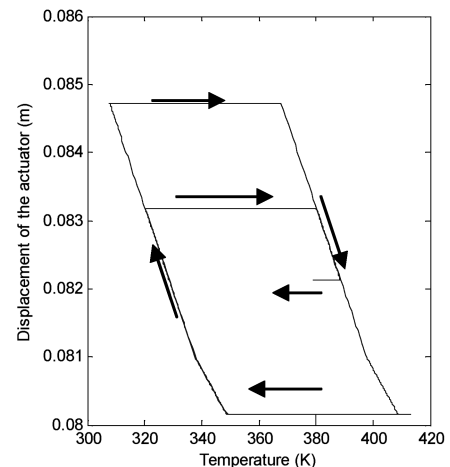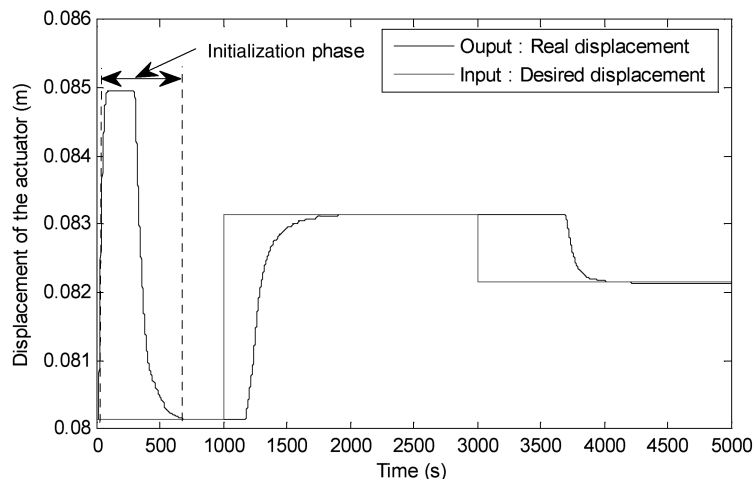

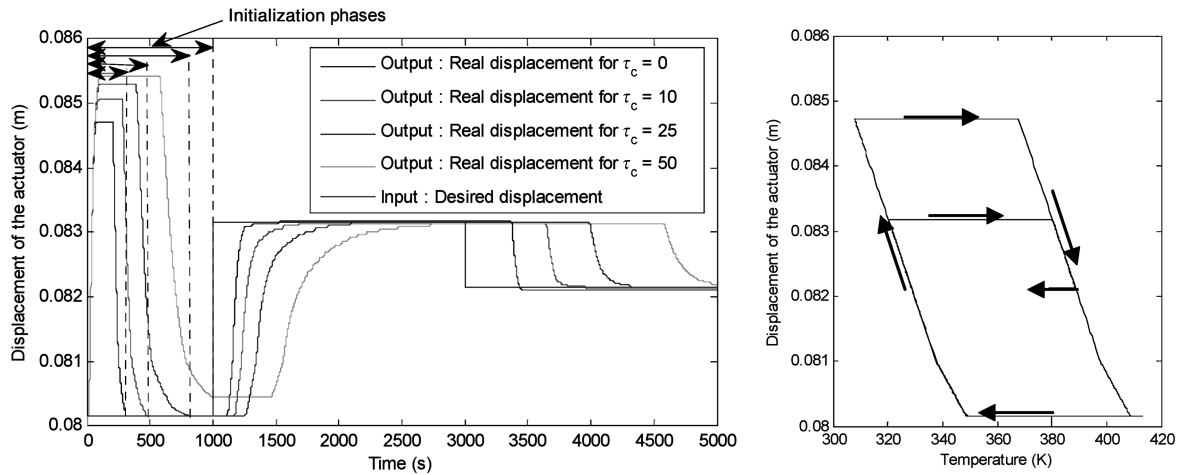**Fig. 12 Displacement of the actuator vs time with the ZN method.**

Fig. 13   Actuator displacement vs time with the IMC method for several τ_c.

the inertia of the system created by the SMA model. The variable gain adjusts the controller as a function of the deflection value entered as the input (block 1 in Fig. 1). Results expressed in terms of actuator displacement variation with time are represented in Fig. 16.

III.   Results and Discussion

Three different types of simulations, one with a step input and a constant α and two with a step input and a sinusoidal α, were performed to validate the controller design (two located in the controller block and one in the SMA block) for the following airflow conditions: Mach number $M = 0.2$, temperature $T = 288.15$ K, and Reynolds number $Re = 2.29 \times 10^6$. The point at which the actuator acts was located at 36% of the chord of the airfoil. The results obtained from these three types of simulations are represented and discussed in terms of airfoil deflections and transition point positions vs time in Secs. III.A–III.C. Three phases are present in these simulations: the initialization phase, the first deflection, and the second deflection. Details of the controller shown in block 3 are given in Fig. 17.

A.   First Simulation Type

During the first simulation, the angle of attack $\alpha = 0$ deg, whereas the airfoil deflection time variation is as follows: 1) from $t = 0$ to 500 s, the deflection remains at 0 mm; 2) from $t = 500$ to 1000 s, the deflection varies from 0 to 20 mm; and 3) from $t = 1000$ to 1500 s, the deflection varies from 20 to 10 mm.

Results are shown in Fig. 18.

Initialization phase: During the initialization phase, more precisely, during the first 500 s, the airfoil deflection input remains at 0 cm. It is seen that, during the first 200 s, the input is different from the output. During this time period of 200 s, the SMA has to go through both the transformation and cooling phases (see Fig. 6). This time period can not be avoided as it is intrinsic to the SMA and actually lasts 200 s. The control can not be achieved until the working point has reached the end of the cooling phase. Following this 200 s time period, it is seen that the transition point position and the airfoil deflection are well controlled, as both of them match well with the input. The transition point position was found to be at 31% of the chord by use of the transition point position algorithm (block 2 in

Fig. 1). A precision of 0.03% for the airfoil deflection and of 0.04% for the transition point position was found.

First airfoil deflection: At $t = 500$ s, a deflection from 0 to 2 cm is enforced, which corresponds to the displacement of the transition point position from 31 to 38% of the chord according to the algorithm described in [8]. The transition point and the deflection are controlled efficiently, as the time response is fast. Even though there is an overshoot, the time response and the precision are satisfactory for both the airfoil deflection and the transition point position. Aprecision of 0.5% for the airfoil deflection and of 0.02% for the transition point position is found. The time response is 56 s for the deflection.

Second airfoil deflection: At $t = 1000$ s, a second airfoil deflection from 2 to 1 cm is given, which corresponds to a displacement of the transition point position between 38 and 33%. The system time response and the precision are satisfactory. A precision of 4.7% for the deflection and of 1.5% for the transition point position are obtained. The time response is 53 s for the airfoil deflection.

B.   Second Simulation Type

In this simulation, the angle of attack is modeled as a sinus function with a 2 deg amplitude and with a frequency of 0.01 rad/s, whereas the airfoil deflection varies with time as follows: 1) from $t = 0$ to 500 s, the deflection remains at 0 mm; 2) from $t = 500$ to 1000 s, the deflection varies from 0 to 20 mm; and 3) from $t = 1000$ to 1500 s, the deflection varies from 20 to 10 mm.

The choice of the sinusoidal wave input for the angle of attack is justified by the fact that it corresponds to the small variations of the angle of attack around 0 deg in the cruise regime, where the angle of attack may be continuously varying. The obtained results are shown in Fig. 19.

It was found that the airfoil deflection is well controlled. The variation of the angle of attack in the second simulation with respect to its variation in the first simulation has no influence on the airfoil deflection control, as this airfoil deflection remains the same as during the first simulation. Only the transition point position oscillates and varies continuously due to the angle of attack sine wave variation. The transition point position is very sensitive to small

Table 1   Comparison of desired displacement with the ZN and IMC methods

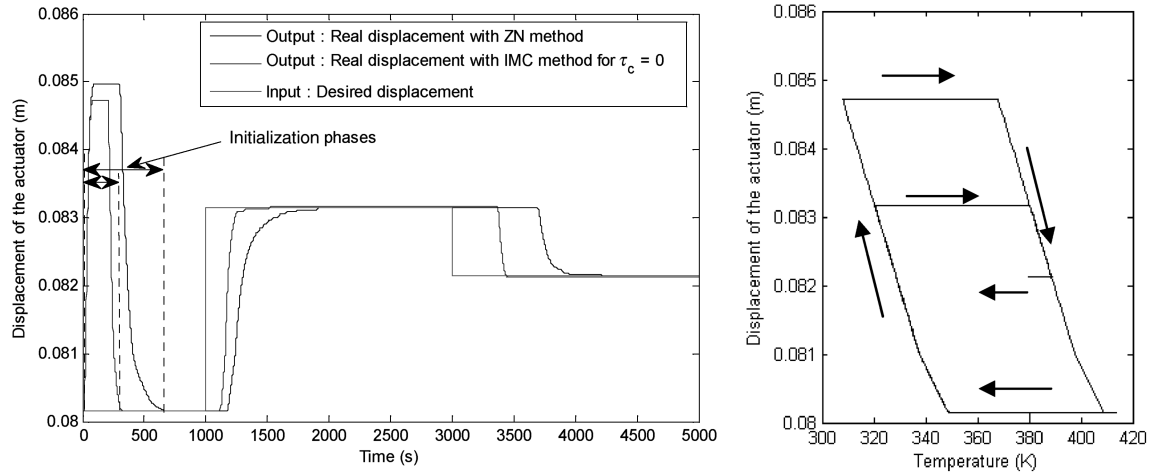|	Desired displacement with the ZN method		Desired displacement with the IMC method	
	Precision, %	Time response, s	Precision, %	Time response, s
Initialization phase	0.12	681	0.07	297
First step	0.02	374	0.09	208
Second step	0.03	748	0.23	381

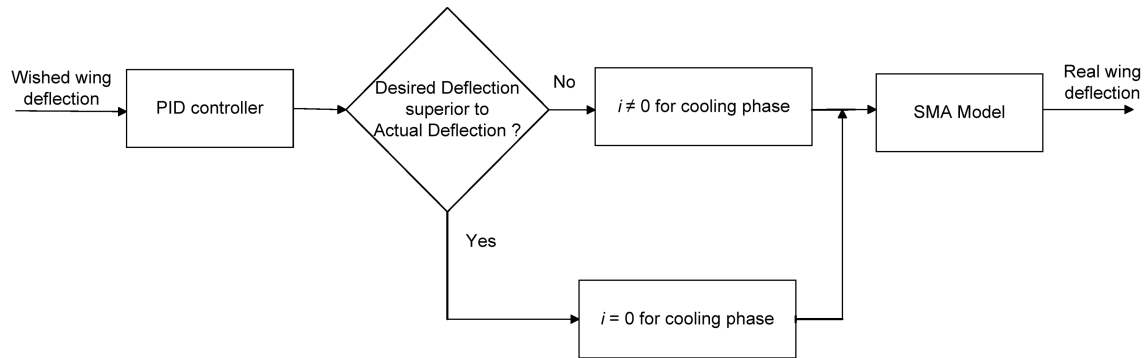**Fig. 14   Displacement of actuator vs time with the ZN and IMC methods.**

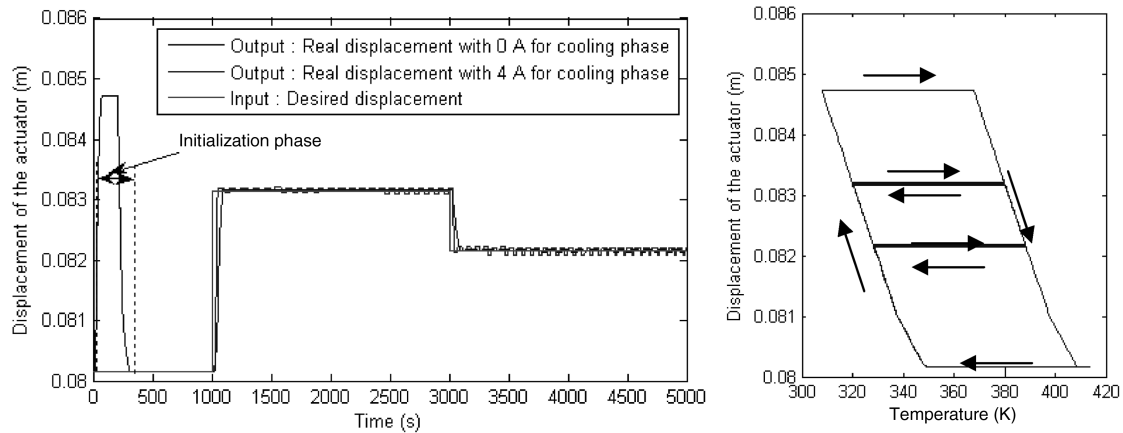**Fig. 15   Algorithm for SMA control improvement.**

Fig. 16   Displacement of the actuator vs time with the new algorithm.

variations of the angle of attack (see Figs. 4–6), which explains the oscillations of the transition point position in Fig. 19.

Initialization phase: During the first 500 s, the input deflection remains at 0 cm. During this phase, the transition point position (as the output) does not fit its input, due to the nonlinear behavior of the SMA. After the 200 s of initialization, the transition point position control is well achieved. The position of the transition point varies very much, from 7 to 75% of the airfoil chord; it fills the whole range of values accepted for the transition point. We found a precision of 0.03% for the deflection and of 0.04% for the transition point position.

First deflection: At $t = 500$ s, a deflection from 0 to 2 cm is enforced. A small overshoot is seen in Fig. 18. A precision of 0.5%

for the airfoil deflection and of 0.12% for the transition point position is found. The time response is 56 s for the airfoil deflection.

Second deflection: At $t = 1000$ s, a deflection from 2 to 1 cm is given to the airfoil. A precision of 4.7% for the airfoil deflection and of 0.02% for the transition point position are found. The time response is 53 s for the airfoil deflection.

C.   Third Simulation Type

The goal of this third simulation is to highlight that changing the shape of the airfoil concretely allows the displacement of the transition point position toward the trailing edge. In this simulation, the angle of attack is modeled as sinusoidal functions with a 2 deg
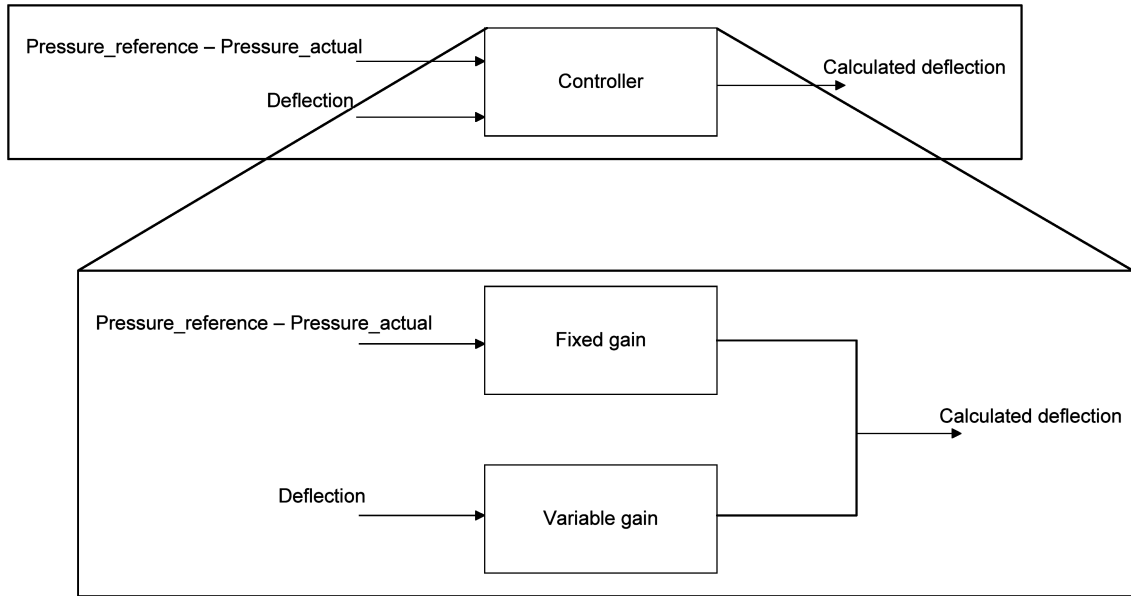
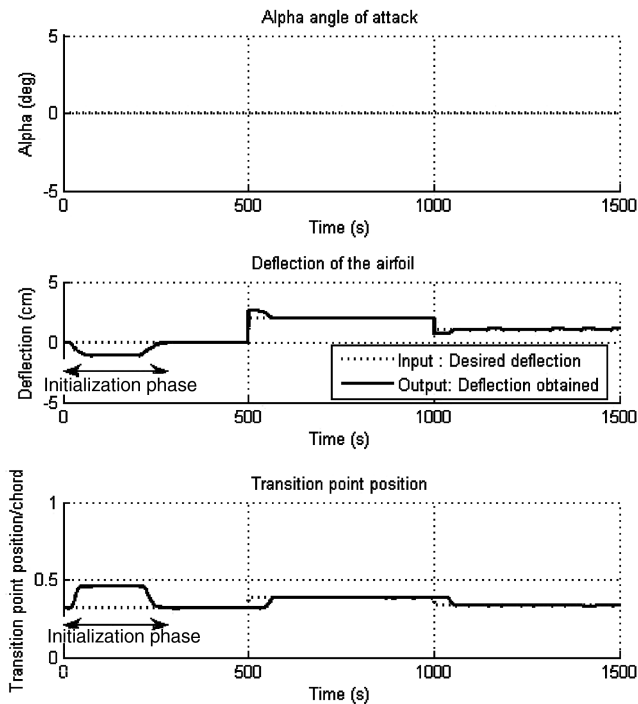Fig. 17   Details of block 3: controller.

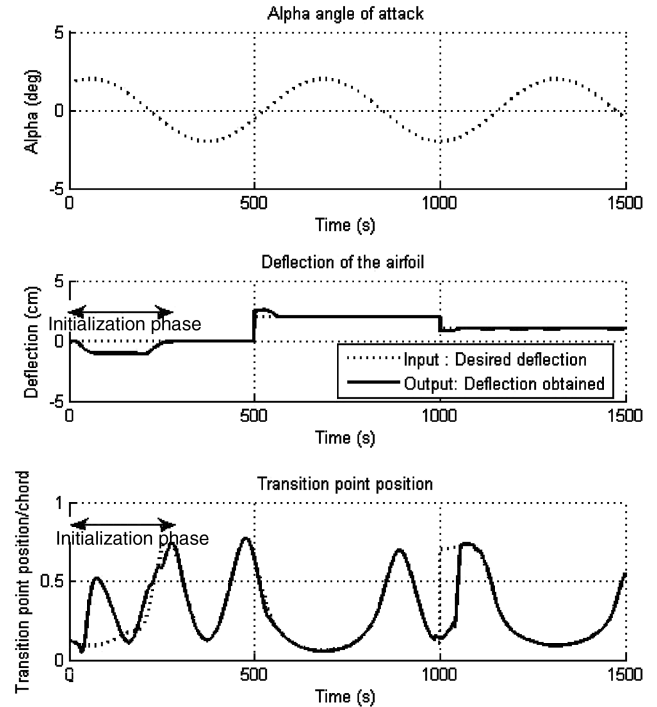Fig. 18   First simulation type results.

Fig. 19   Second simulation type results.

amplitude and a frequency of 0.01 rad/s, whereas the deflection has the same frequency but is in antiphase to the alpha oscillations and has amplitudes of 0.5 cm. Results are shown in Fig. 20.

Initialization phase: During this phase, the transition point position and the deflection do not fit the respective inputs, due to the nonlinear behavior of the SMA. After the 200 s of initialization, the control is well achieved. The position of the transition point varies from 9 to 55% of the chord. The deflection varies from −1.5 to 0 cm.

After the initialization phase: During the next 1250 s, the control is satisfactory. It is noticed that the change of the shape of the airfoil allows us to move the transition point position toward the trailing edge. For small negative angles of attack, an amplitude of the deflection of 0.5 cm is the optimum for maintaining the transition point the furthest to the trailing edge. From Figs. 6 and 20, it can be seen that for positive angles of attack the transition point position is minimally influenced by the deflection of the airfoil shape.

IV.   Conclusions

This paper presents an easy implementation of controlling the deflection on a morphing wing airfoil equipped with actuators, sensors, and flexible skin, which ultimately has an effect on the transition point position. The realization of the control has been carried out in two steps. The first step was to control the SMA block (block 4 in Fig. 1). The SMA has a nonlinear behavior with a slow dynamic. The IMC method was preferred to the ZN method as it provided better results. Once the closed loop inside the SMA block has been controlled, then the whole closed loop is controlled. The whole closed loop has a very fast dynamic, because of the real-time controller located in the determination of the pressure coefficients vs chord and transition point position block (block 2 in Fig. 1). For this reason, a controller block (block 3 in Fig. 1) is necessary. The proportional gain reduces the inertia of the system created by the
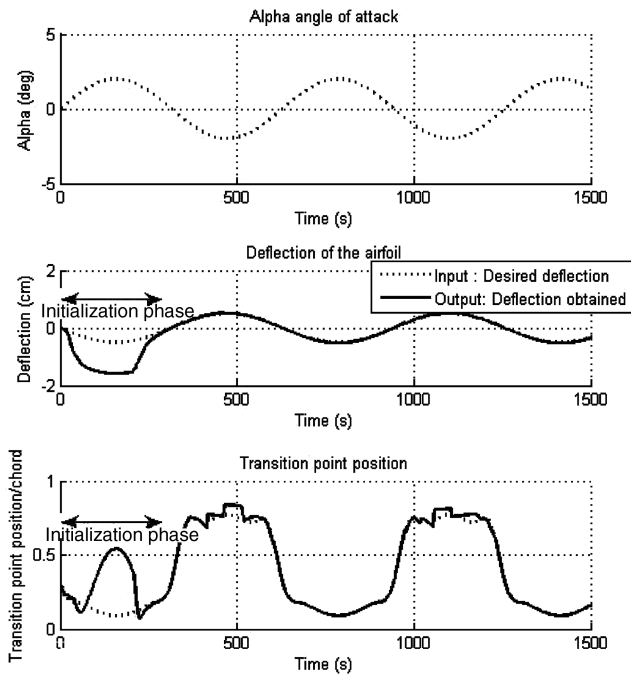
Fig. 20   Third simulation type results.

SMA model. The variable gain adjusts the control as a function of the deflection value entered as the input (block 1 in Fig. 1).

The simulations validated our choice of design, as fast and precise responses are obtained. The main advantage of this new and original method is its simplicity and its incorporation in experimental applications, such as in the controller of a morphing wing model. It is the first time that such a controller design concept is presented.

Acknowledgments

References

[1] Munday, D., Jacob, J. D., Hauser, T., and Huang, G., "Experimental and Numerical Investigation of Aerodynamic Flow Control Using Oscillating Adaptive Surfaces," AIAA Paper 2002-2837, 2002.
[2] Wadehn, W., Sommerer, A., Lutz, T., Fokin, D., Pritschow, G., and Wagner, S., "Structural Concepts and Aerodynamic Design of Shock Control Bumps," ICAS Paper 66R1.1, Sept. 2002.
[3] Sobieczky, H., and Geissler, W., "Active Flow Control Based on Transonic Design Concepts," AIAA Paper 99-3127, 1999.
[4] Martins, A. L., and Catalano, F. M., "Drag Optimization for Transport Aircraft Mission Adaptive Wing," *Journal of the Brazilian Society of Mechanical Sciences and Engineering*, Vol. 25, No. 1, 2003, pp. 1–8. doi:10.1590/S1678-58782003000100001
[5] Powers, S. G., and Webb, L. D., "Flight Wing Surface Pressure and Boundary-Layer Data Report from the F-111 Smooth Variable-Camber Supercritical Mission Adaptive Wing," NASA TM-4789, 1997.
[6] Lee, J.-R., Ryu, C.-Y., Koo, B.-Y., Kang, S.-G., Hong, C.-S., and Kim, C.-G., "In-Flight Health Monitoring of a Subscale Wing Using a Fibre Bragg Grating Sensor System," *Smart Materials and Structures*, Vol. 12, No. 1, Feb. 2003, pp. 147–155. doi:10.1088/0964-1726/12/1/317
[7] Martin, C. A., Bartley-Cho, J. D., and Flanagan, J. S., "Design and Fabrication of Smart Wing Wind Tunnel Model and SMA Control Surfaces," *Conference of Smart Structures and Materials 1999: Industrial and Commercial Applications of Smart Structures Technologies*, Vol. 3674, Society of Photo-Optical Instrumentation Engineers1999, pp. 237–248. doi:10.1117/12.351562
[8] Popov, A., Botez, R. M., and Labib, M., "Transition Point Detection from the Surface Pressure Distribution for Controller Design," *Journal of Aircraft*, Vol. 45, No. 1, 2008, pp. 23–28. doi:10.2514/1.31488
[9] Brailovski, V., Prokoshkin, S., Terriault, P., and Trochu, F. (eds.), *Shape Memory Alloys: Fundamentals, Modeling and Applications*, École de Technologie Supérieure, Montreal, 2003, ISBN 2-921145-42-1.
[10] Song, G., Kelly, B., and Agrawal, B. N., "Active Position Control of a Shape Memory Alloy Wire Actuated Composite Beam," *Smart Materials and Structures*, Vol. 9, No. 5, 2000, pp. 711–716. doi:10.1088/0964-1726/9/5/316
[11] Ziegler, J. G., and Nichols, N. B., "Optimum Settings for Automatic Controllers," *Transactions of the American Society of Mechanical Engineers*, Vol. 64, No. 8, 1942, pp. 759–768.
[12] Rivera, D. E., Morari, M., and Skogestad, S., "Internal Model Control: PID Controller Design," *Industrial and Engineering Chemistry Process Design and Development*, Vol. 25, No. 1, 1986, pp. 252–265. doi:10.1021/i200032a041